JOURNAL OF MOLECULAR SPECTROSCOPY **102**, 320–343 (1983)

High-Resolution Laser-rf Spectroscopy on the $A^2\Pi_{3/2}$–$X^2\Pi_{3/2}$ System of Iodine Oxide (IO)

J. P. BEKOOY, W. LEO MEERTS, AND A. DYMANUS

Fysisch Laboratorium, Katholieke Universiteit, Toernooiveld, 6525 ED Nijmegen, The Netherlands

The rotational spectra of the vibrational bands 2–0, 2–1, and 2–2 of the $A^2\Pi_{3/2}$–$X^2\Pi_{3/2}$ system of the IO radical have been studied at high resolution by molecular-beam laser-excitation spectroscopy. The hyperfine structure could be resolved for the lowest rotational levels and the hyperfine constants eQq_1 and $a + (1/2)(b + c)$ have been determined for both the excited and ground states. Hyperfine splittings within rotational levels of the ground vibrational $X^2\Pi_{3/2}$ state have been studied by a new spectroscopic method: microwave optical double resonance on a state-selected beam. The hyperfine constants eQq_2 and $b - C_I(\lambda - 2)$ of the $v = 0$, $X^2\Pi_{3/2}$ state could be deduced as well. The widths of the rotational levels in the excited $v = 2$, $A^2\Pi_{3/2}$ state have been determined. Apart from the vibrationally dependent predissociation, a predissociation which depends on the rotational state has been observed.

1. INTRODUCTION

Spectroscopy on the ground and first excited electronic states of the halogen monoxides is hindered by instability of these radicals and extensive predissociation in the $A^2\Pi_i$ states. Their possible intermediate role in stratospheric (ClO and BrO) tropospheric (IO) (*1*) photochemistry, which limits the atmospheric abundance of ozone, has raised interest in the past years. The spectra of ClO and BrO have been studied extensively and the spectrum of FO in the gas phase has been observed only recently by laser magnetic resonance (*2*). The $A^2\Pi_{3/2}$–$X^2\Pi_{3/2}$ system of IO has been subject of several investigations. It was first observed in emission by Vaidya (*3*). Coleman *et al.* (*4*) extended the emission spectrum at low dispersion and analyzed the vibrational band system. Durie and Ramsay (*5*) observed the absorption spectrum, and Durie *et al.* (*6*) observed and analyzed the vibrational and rotational structure of the moderately resolved emission spectrum. Vibronic progressions of absorption and emission spectra of IO isolated in an argon matrix were observed by Loewenschuss *et al.* (*7*). The ground vibrational $X^2\Pi_{3/2}$ state of IO was studied by electron resonance spectroscopy in the $J = 3/2$ rotational level by Carrington *et al.* (*8*) and in the $J = 5/2$ level by Brown *et al.* (*9*). Saito (*10*) studied the two lowest rotational transitions in the ground vibrational $X^2\Pi_{3/2}$ state by microwave absorption spectroscopy.

In this paper we report a study on the $A^2\Pi_{3/2}$–$X^2\Pi_{3/2}$ system of the IO radical by high-resolution laser-rf spectroscopy. The hyperfine interaction in the excited state and the hyperfine Λ-doublet splittings in the ground state have been observed for the first time. Two distinct experimental methods have been used: molecular-beam laser excitation (MBLE) and microwave optical double resonance on an electrically state-

0022-2852/83 $3.00

selected beam (MODRES). The latter method is a new and powerful technique that combines the high resolution of microwave spectroscopy on molecular beams with the high sensitivity of state-resolved detection by laser-induced fluorescence.

The rotational spectra of the vibrational bands 2–0, 2–1, and 2–2 of the $A^2\Pi_{3/2}$–$X^2\Pi_{3/2}$ transition have been studied using the MBLE method. Hyperfine structures could be resolved for the lowest rotational transitions. The effective rotational constant B, the centrifugal distortion constant D, the electric quadrupole coupling constant eQq_1, and the magnetic hyperfine constant $a + (1/2)(b + c)$ have been determined for the $v = 2$ level of the $A^2\Pi_{3/2}$ state and the $v = 0$, 1 and 2 levels of the $X^2\Pi_{3/2}$ state. For the ground state, vibrational constants and vibrational series expansion coefficients for the rotational constants have been derived.

The widths of the rotational levels in the excited $v = 2$, $A^2\Pi_{3/2}$ state have been determined from the optical excitation spectra. Apart from the predissociation, which varies with vibrational level and is commonly observed for the $A^2\Pi_i$ states of the halogen monoxides, a rotationally dependent predissociation has been observed as well, indicating additional gyroscopic interaction with unbound states.

Hyperfine splittings within rotational levels of the ground vibrational $X^2\Pi_{3/2}$ state have been further studied by the MODRES method. From these measurements the nonaxial electric quadrupole coupling constant eQq_2 and the effective magnetic hyperfine constant $b - C_I(\lambda - 2)$ could be determined for the $v = 0$ level of the $X^2\Pi_{3/2}$ ground state.

For the interpretation of the observed spectra, theory for $^2\Pi$ states has been employed. The final constants have been determined from a merged least-squares fit to all data from the present investigation, combined with flame emission data of Durie *et al.* (*6*) and microwave absorption data of Saito (*10*).

2. EXPERIMENTAL METHODS

The two configurations of the spectrometer used in the investigation of IO are shown in Fig. 1. In case of the MBLE experiments the laser beam intersects the

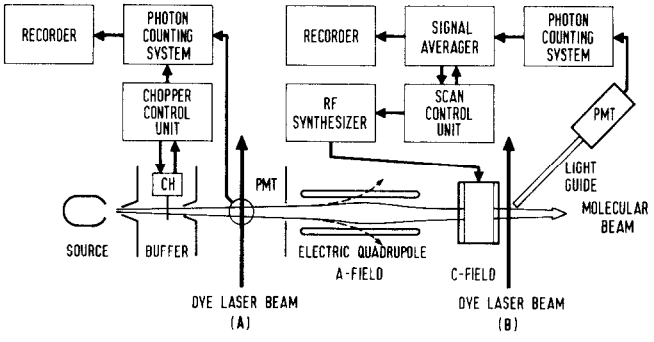

FIG. 1. Outline of the spectrometer. The dye laser beam intersects the molecular beam orthogonally either at position (A), in the case of the molecular-beam laser-excitation (MBLE) configuration, or at position (B), in the case of the microwave optical double resonance on an electrically state-selected beam (MODRES) configuration. CH: beam chopper; PMT: photomultiplier.

molecular beam at position (A) and for the MODRES experiments at position (B). With the MBLE method, transitions to excited electronic states can be studied by means of detection of the subsequently emitted laser-induced fluorescence (LIF). The spectral resolution is usually limited (apart from the natural linewidth) by the residual Doppler broadening (in the order of 10 MHz) determined by the degree of molecular beam collimation.

The MODRES method is a new and powerful technique which combines high resolution with high sensitivity. A microwave optical double-resonance arrangement is used, in which transitions induced by microwave radiation between certain levels in the electronic ground state are detected as a change in the LIF intensity. State selection is required in this method because states involved in microwave transitions are almost equally populated. This is achieved by an electrostatic quadrupole field, called A field in analogy with the molecular-beam electronic-resonance (MBER) method. In the experimental setup (Fig. 1) the molecular beam produced by the source is state selected by the A field and detected by LIF. The microwave or radio-frequency (rf) transition is induced in the C field located between the A field and the intersection of the laser and molecular beam at position (B). The laser frequency is kept fixed at a specific optical excitation transition and the LIF intensity is monitored. In this way the laser monitors the number of molecules in a specific energy level of the ground electronic state. The A field deflects molecules according to their quantum states, towards the molecular beam axis (positive Stark effect, trajectories indicated by solid lines in Fig. 1) or away from it (negative Stark effect, dashed line trajectories). If in the C field a transition from a state transmitted to a state rejected by the A field is induced by radio-frequency (rf) (or microwave) radiation, a decrease (flop-out) in the LIF intensity will occur if the initial state is probed by the laser (double-resonance condition). Alternatively, an increase (flop-in) will occur if the final state is probed by the laser. As illustration a schematic energy level diagram is given in Fig. 2, in which two of the double-resonance transitions observed are indicated. The Λ-doublet components of the hyperfine levels in the ground state with symmetry − and + exhibit mainly positive and negative Stark effects, respectively. The LIF detection was performed on the $A^2\Pi_{3/2}$–$X^2\Pi_{3/2}$, 2–0, $P(9/2)$, $F' = 5 \leftarrow F'' = 6$ (+ ← − and − ← +) transition. The hyperfine rf transitions $6_- \leftarrow 5_+$ (flop-out) and $6_+ \leftarrow 5_-$ (flop-in) within the $J = 9/2$ rotational level of the $v = 0$, $X^2\Pi_{3/2}$ ground state have been observed.

The MODRES method provides a high spectral resolution (in the order of 10 kHz), because the linewidths are only determined by the transit time of the molecules through the C-field transition region. The linewidths in the double-resonance rf spectra do not depend on the much broader linewidths of the LIF transitions. The state-resolved LIF detection improves the sensitivity by several orders of magnitude compared to total beam detection, as applied in conventional molecular-beam electric resonance (MBER) (for a review see, e.g., Ref. (*11*)). Since the laser excitation is state selective, the signals and noise originate only from the molecular states of interest, aside from spurious background due to straylight and photodetector noise. Furthermore, the double-resonance condition makes identification of complicated optical spectra easier than in the MBLE method. The absence of the state-analyzing B field

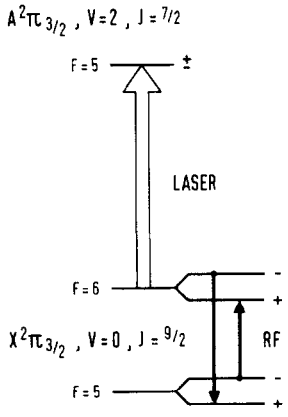

FIG. 2. Schematic energy level diagram, in which two of the double-resonance transitions observed are indicated.

of MBER allows detection of both flop-in and flop-out signals. Inclusion of this *B* field is only necessary in the (rare) case the laser excitation cannot accomplish full state analysis because the two states connected by the microwave radiation fall within its spectral resolution. The drawback of the MODRES method is its restriction to transitions between (ground) states complying with rather strict state-selection rules.

The present MODRES method resembles the molecular-beam magnetic resonance with laser detection as introduced by Grundevik *et al.* (*12*) and the molecular-beam laser-induced fluorescence resonance as introduced by Rosner *et al.* (*13*). The first method employs inhomogeneous magnetic *A* and *B* fields and applies to atoms or molecules with magnetic dipole moments. In the method of Rosner *et al.* the *A* field is replaced by the intersection with another beam from the same laser, which produces state labeling by depleting the population of a specific energy level in the ground electronic state by means of optical pumping. This method is not restricted to polar species; however, it applies only if sufficient optical pumping can be achieved.

The IO radical was produced by the reaction of atomic oxygen with iodine molecules:

$$O(^3P) + I_2(^1\Sigma_g^+) \rightarrow IO(^2\Pi) + I(^2P). \quad (1)$$

This reaction was found to be twice as efficient in beam formation as the reaction of atomic oxygen with methyl iodide (CH_3I) used by Saito (*10*). The molecular beam of IO radicals was formed in a reaction source analogous to the source used in the experiments on the hydroxyl (OH) radical (*14*). The optimized design is shown in Fig. 3. The source consists of pyrex tubes, with inner diameters 4 and 10 mm, that are wrapped around with heating wires. The temperature was kept at 400 to 500 K to maintain the iodine molecules in vapor phase. Atomic oxygen is produced by a microwave discharge at 2.45 GHz, located off-axis to eliminate stray light along the beam direction. About 10% dissociation to atomic oxygen was obtained at a power dissipation of 75 to 150 W. The iodine molecules are injected into the reaction zone via an orifice of 2-mm diameter. The end of the source, in front of the skimmer, has

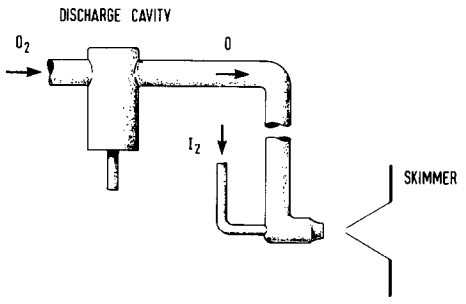

FIG. 3. Diagram of the reaction source for IO molecular beam production.

been contracted to an optimized diameter of 6 mm. The efficiency of IO beam formation is strongly dependent on this diameter and increased by an order of magnitude compared to an uncontracted 10-mm tube. The molecular beam is formed by a conical skimmer with an aperture of 2 mm located about 12 mm downstream from the source. Typical pressure in the source chamber (pumped by a 500-m^3/hr Roots pump) was 4×10^{-2} mbar. The iodine consumption was about 2.5 g/hr. Various compounds are deposited on the inner wall of the reaction tube and on the skimmer. This results in clogging and necessitates cleaning after about 7 hr of operation. Yellow-green chemiluminescence emanating from the reaction zone proved to be helpful to adjust the source conditions.

The laser radiation for the experiments has been produced by a tunable single-frequency cw dye laser (Coherent Radiation 599-21). The gain medium is a solution of Stilbene 3 (420) dye in ethylene glycol (0.75 g/liter) and is pumped by the uv lines from an Ar-ion laser (Spectra Physics 171-UV). The dye laser has been equipped with coumarin 102 (480) optics. The maximum single-frequency output power in the region 445 to 475 nm decreases from 100 to 35 mW, respectively, at a pumping power of 1.7 W. The dye laser power can be stabilized by an external feedback system. The effective spectral bandwidth due to residual jitter of the laser frequency is 3 MHz. An external scanning ramp generator provides a linear up or down going ramp to drive the scan controls of the dye laser.

A thermally stabilized confocal Fabry-Pérot interferometer (Burleigh CFT-500), with a free spectral range of 150 MHz, is used to monitor the dye laser frequency. The transmission peaks in the fixed mode of operation furnish relative frequency markers if the laser is scanned. In the MODRES experiments the interferometer is used in the scanning mode to monitor eventual drifts in the dye laser frequency, which are subsequently compensated by manual adjustment of the scan controls. Calibration of the free spectral range has been performed against known splittings in the IO ground state, with an accuracy of 1×10^{-4}. The dye laser was scanned across transitions terminating in the same hyperfine level of a rotational state in the excited $v = 2$, $A^2\Pi_{3/2}$ state, but originating from different hyperfine levels in rotational states in the $v = 0$, $X^2\Pi_{3/2}$ ground state whose energy separation is known from the data of Saito (*10*). The calibration scans spanned intervals of 50 and 70 GHz, covering

hyperfine structures of the rotational transitions $Q(3/2)$ to $P(5/2)$ and $Q(5/2)$ to $P(7/2)$, respectively.

The absolute frequency of the dye laser is determined using a wavelength meter, which compares the dye laser wavelength with the accurately known wavelength of a reference laser. Its principle is based on a Michelson interferometer with electronic counting of interference fringes (*15–17*). The wavelength meter incorporates variation of the optical path length inside a vacuum chamber (eliminating elaborate dispersion corrections), phase-locked 100-fold fringe frequency multiplication (for fringe interpolation), and a single-frequency HeNe reference laser with thermal frequency stabilization (*18, 19*). The wavelength of this reference HeNe laser was determined regularly by measuring the wavelength of the dye laser tuned to the Lamb-dip of the transition at 436 nm of the ^{198}Hg secondary standard. The absolute wavelength of this transition has been determined accurately relative to the ^{86}Kr primary standard (*20*). By this intrinsic method of calibration, any eventual systematic errors are eliminated. The absolute accuracy of the digital wavelength meter is 1.2×10^{-7}, throughout the visible region.

An outline of the spectrometer is given in Fig. 1. In the MBLE experiments the dye laser beam intersects the molecular beam orthogonally at position (A) (distance from the source is 30 cm). The IO beam is modulated by a mechanical chopper to eliminate off-phase background signals. The LIF is collected by an optical system consisting of aspherical lenses and a concave spherical mirror, in a direction perpendicular to both beams, with an angular efficiency of 20–25%. The collected LIF is transmitted to the photocathode of a photomultiplier (EMI 9635) and monitored by a photon-counting system (ORTEC-Brookdeal 5C1). The vibrational bands of the optical spectra are located at 445 nm (2–0), 459 nm (2–1), and 473 nm (2–2). The collected light is passed through a spectral filter (Schott CG 495, thickness 3 mm) with cutoff wavelength at 495 nm, to discriminate against scattered laser light. The signal is registered on a dual-channel chart recorder, together with laser frequency marks provided by the Fabry–Pérot reference interferometer. The strongest lines in the IO spectrum were 8000 counts/sec, yielding a signal to noise ratio of about 40 at a counting time of 1 sec. The spectral resolution is determined by a convolution of the natural linewidth and the instrumental limitations imposed by residual Doppler broadening, laser frequency jitter, transit time broadening, and wavefront curvature broadening (*21, 22*). Under the experimental conditions (full angular divergence of the molecular beam is 20 mrad, laser frequency jitter is 3 MHz, diameter of the laser beam is 5 mm, and full angular divergence of the laser beam is 0.5 mrad), the Gaussian profile from instrumental broadening is estimated to have a width (FWHM) of 10–20 MHz. The linewidths observed in the IO spectrum were always dominated by the natural linewidths. A typical spectral recording of the hyperfine structure of the $Q(3/2)$ rotational transition of the 2–0 band is shown in Fig. 4.

For the MODRES experiment (Fig. 1) with laser intersection at position (B), the laser frequency is tuned to a specific optical excitation transition in the 2–0 band. In this case the LIF is collected by a light guide (Schott LST) at an angle of 45° with both the laser and molecular beam, with an angular efficiency of about 2%. The collected LIF is detected by a cooled photomultiplier (EMI 9863/350) connected to

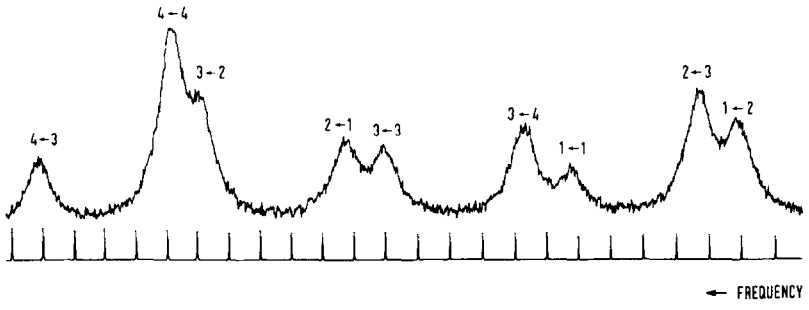

FIG. 4. Spectral recording of the $Q(3/2)$ rotational transition in the 2–0 vibrational band of the $A^2\Pi_{3/2}$–$X^2\Pi_{3/2}$ system of IO (at 445.04175(5) nm), observed by MBLE. The hyperfine structure transitions are indicated as $F' \leftarrow F''$ (+ ← − and − ← +). Frequency intervals between two subsequent transmission peaks of the interferometer given in the lower trace are 149.605(15) MHz. The natural linewidth is 148(12) MHz (FWHM).

the photon-counting system. The double-resonance signal stimulated by the rf radiation in the C field is observed by monitoring the LIF intensity versus the rf frequency. The rf is generated by a programmable rf synthesizer (Hewlett–Packard 8660 B). A signal averager (Hewlett–Packard 5480 B), inferfaced with the scan control unit, has been employed. For searching over wide frequency regions, artificial line broadening by random frequency modulation of the rf synthesizer has been employed (*14*). After preliminary location of a transition, an accurate frequency determination is performed at normal resolution.

Several hyperfine transitions within rotational levels of the $v = 0$, $X^2\Pi_{3/2}$ ground state of IO have been studied. The hyperfine levels are split into two closely spaced Λ-doublet states with different symmetry, which exhibit mainly linear Stark effect. The large dipole moment of 2.5 D (*23*) allows state selection for the lower rotational levels at moderate voltages. The intensities of the double-resonance transitions were about 15 counts/sec. The main reason for the strong reduction of the signals is the larger distance from the source (145 cm). In most cases 32 rf scans (each scan took 1 min at 1 sec time constant) were averaged, yielding a final signal to noise ratio in the order of two. Although the obtainable linewidths are in principle 10 kHz (the length of the C field is 5 cm), this limit is not reached for the low J states of IO. This is due to the residue of the compensated Earth's magnetic field, which causes broadening of transitions in the paramagnetic $X^2\Pi_{3/2}$ state. A typical spectral recording of hyperfine transitions within the $J = 9/2$ rotational state is shown in Fig. 5. A schematic energy level diagram corresponding to these double-resonance transitions has been given in Fig. 2.

3. THEORY

Both the observed excited $A^2\Pi_{3/2}$ and ground $X^2\Pi_{3/2}$ state belong to $^2\Pi$ doublets. The ground $X^2\Pi$ doublet is known to be inverted with a large spin–orbit separation

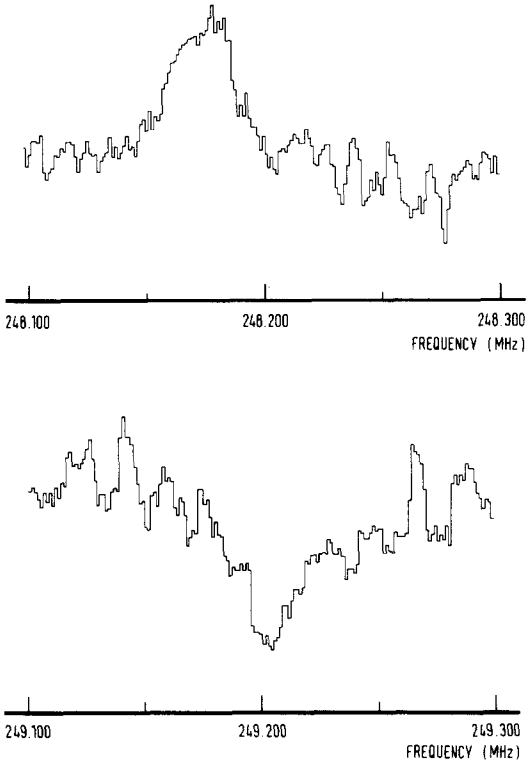

FIG. 5. Spectral recording of the hyperfine transitions within the $J = 9/2$ rotational level of the $v = 0$, $X^2\Pi_{3/2}$ ground state of IO, observed by MODRES. The LIF detection was performed on the $A^2\Pi_{3/2}$–$X^2\Pi_{3/2}$, 2–0, $P(9/2)$, $F' = 5 \leftarrow F'' = 6$ ($+ \leftarrow -$ and $- \leftarrow +$) transition. The hyperfine rf transitions $6_+ \leftarrow 5_-$ (flop-in signal) and $6_- \rightarrow 5_+$ (flop-out) have been observed.

and can be described by a coupling scheme close to Hund's case (a). The Hamiltonian for a diatomic molecule in an electronic $^2\Pi$ state in absence of external fields may be written in a formal way as

$$H = H_{ev} + H_F + H_{hf}. \tag{2}$$

Here H_{ev} represents the part concerning the purely electronic and vibronic term energies, H_F contains the rotational energy and the fine-structure interactions, and H_{hf} describes the hyperfine interactions. The theory used for the interpretation of the spectra incorporates two modifications of the theory derived in detail elsewhere (*14, 24, 25*). First, for H_F the effective Hamiltonian for the rotational and spin structure of a given isolated vibronic state derived by Brown *et al.* (*26*) has been adopted. Their treatment is to be preferred since the resulting effective Hamiltonian is uncoupled from other electronic and vibronic states. The matrix elements are evaluated using an expansion of the Hamiltonian in $\mathbf{N}^2$ instead of $\mathbf{R}^2$ as done in Ref. (*14, 24, 25*). The second modification concerns the phase factors for the off-diagonal matrix elements

between the $^2\Pi_{1/2}$ and $^2\Pi_{3/2}$ states. The phase convention now employed is in accordance with the direct tensor method of Brown and Howard (*27*).

A basis set of Hund's case (a) wavefunctions, symmetrized with respect to reflection in a plane through the molecular axis, is used ($n = X, A$ labels the electronic states):

$$|n^2\Pi_\Omega^\pm vJ\rangle = (|nvJ\Lambda\Sigma\Omega\rangle \pm (-1)^{J-1/2}|nvJ - \Lambda - \Sigma - \Omega\rangle)/2^{1/2}. \quad (3)$$

The total wavefunctions $|n^2\Pi_\Omega^\pm vJIF\rangle$ including the nuclear spin are constructed as a product of the functions $|n^2\Pi_\Omega^\pm vJ\rangle$ and the nuclear spin functions $|IM_I\rangle$ according to the coupling scheme $\mathbf{F} = \mathbf{J} + \mathbf{I}$. The matrix elements for the part H_F of the effective Hamiltonian are given by

$$\langle n^2\Pi_{1/2}^\pm vJIF|H_F|n^2\Pi_{1/2}^\pm vJIF\rangle$$

$$= -\frac{1}{2}A_{nv} - \frac{1}{2}A_{Dnv}(X+2) - \gamma_{SRnv} + B_{nv}(X+2) - D_{nv}(X+1)(X+4) + H_{nv}$$

$$\times (X+1)(X^2+8X+8) \pm (-1)^{J-1/2}\frac{1}{2}p_{nv}(J+1/2) \pm (-1)^{J-1/2}q_{nv}(J+1/2), \quad (4)$$

$$\langle n^2\Pi_{3/2}^\pm vJIF|H_F|n^2\Pi_{3/2}^\pm vJIF\rangle$$

$$= \frac{1}{2}A_{nv} + \frac{1}{2}A_{Dnv}X + B_{nv}X - D_{nv}X(X+1) + H_{nv}X(X+1)(X+2), \quad (5)$$

$$\langle n^2\Pi_{1/2}^\pm vJIF|H_F|n^2\Pi_{3/2}^\pm vJIF\rangle$$

$$= \frac{1}{2}\gamma_{SRnv}X^{1/2} - B_{nv}X^{1/2} + 2D_{nv}X^{1/2}(X+1) - H_{nv}X^{1/2}(X+1)(3X+4)$$

$$\mp (-1)^{J-1/2}\frac{1}{2}q_{nv}X^{1/2}(J+1/2), \quad (6)$$

where $X = (J+1/2)^2 - 1 = (J-1/2)(J+3/2)$. If two signs are given, the upper and lower sign is appropriate for the states with symmetry $+1$ and -1, respectively. Expressions for higher-order terms can be found in a paper by Amiot *et al.* (*28*). The contributions included in the expressions above arise from the spin–orbit coupling (A) with centrifugal distortion (A_D), the spin–rotation interaction (γ_{SR}), the rotational energy (B) with centrifugal distortion to first (D) and second-order (H), and the Λ-splitting (p and q). The matrix elements for the hyperfine part H_{hf} of the Hamiltonian are given by

$$\langle n^2\Pi_{1/2}^\pm vJIF|H_{hf}|n^2\Pi_{1/2}^\pm vJ'IF\rangle$$

$$= G(JJ'IF)\left\{(-1)^{J'-1/2}\begin{pmatrix} J & 1 & J' \\ -1/2 & 0 & 1/2\end{pmatrix}\left[a_{nv} - \frac{1}{2}(b_{nv}+c_{nv}) + \delta_{JJ'}2C_{1nv}X\right]\right.$$

$$\left. \mp \begin{pmatrix} J & 1 & J' \\ -1/2 & 1 & -1/2\end{pmatrix}d_{nv}/2^{1/2}\right\} + Q(JJ'IF)(-1)^{J'-1/2}\begin{pmatrix} J & 2 & J' \\ -1/2 & 0 & 1/2\end{pmatrix}\frac{1}{4}eQq_{1nv}, \quad (7)$$

$$\langle n^2\Pi^{\pm}_{3/2} vJIF|H_{\rm hf}|n^2\Pi^{\pm}_{3/2} vJ'IF\rangle$$

$$= G(JJ'IF)(-1)^{J'-3/2}\begin{pmatrix} J & 1 & J' \\ -3/2 & 0 & 3/2\end{pmatrix}\left[a_{nv} + \frac{1}{2}(b_{nv} + c_{nv}) + \delta_{JJ'}(2/3)C_{1nv}X\right]$$

$$+ Q(JJ'IF)(-1)^{J'-3/2}\begin{pmatrix} J & 2 & J' \\ -3/2 & 0 & 3/2\end{pmatrix}\frac{1}{4}eQq_{1nv}, \quad (8)$$

$$\langle n^2\Pi^{\pm}_{1/2} vJIF|H_{\rm hf}|n^2\Pi^{\pm}_{3/2} vJ'IF\rangle = G(JJ'IF)(-1)^{J'-1/2}\begin{pmatrix} J & 1 & J' \\ -3/2 & 1 & 1/2\end{pmatrix}b_{nv}/2^{1/2}$$

$$\mp Q(JJ'IF)\begin{pmatrix} J & 2 & J' \\ -3/2 & 2 & -1/2\end{pmatrix}\frac{1}{4}eQq_{2nv}/6^{1/2}, \quad (9)$$

where

$$G(JJ'IF) = [(2J+1)(2J'+1)I(I+1)(2I+1)]^{1/2}(-1)^{J+I+F}\begin{Bmatrix} F & J & I \\ 1 & I & J'\end{Bmatrix}$$

and

$$Q(JJ'IF) = \left[\frac{(2J+1)(2J'+1)(I+1)(2I+1)(2I+3)}{I(2I-1)}\right]^{1/2}(-1)^{J+I+F}\begin{Bmatrix} F & J & I \\ 2 & I & J'\end{Bmatrix}.$$

These expressions[1] contain the magnetic hyperfine (a, b, c, and d), the nuclear spin–rotation (C_1), and the electric quadrupole (eQq_1 and eQq_2) coupling constants. It should be noted that the sign in front of eQq_2 is opposite of that used before (*24, 25*), so consequently the eQq_2 value reverses sign. In view of the confusion on the sign of eQq_2, a separate discussion on this topic is given in the appendix.

The presently available data on the IO spectrum do not allow for an independent determination of all the molecular constants occurring in the effective Hamiltonian. At first, the nearly total correlation among A_{Dnv} and γ_{SRnv} is removed, as usually, by a transformation of the Hamiltonian, which eliminates γ_{SRnv} and leads to the effective parameters (*26*)

$$(T_{ne} + G_{nv})^{\rm eff} = T_{ne} + G_{nv} - \frac{1}{2}\gamma_{SRnv}\lambda_{nv}/(\lambda_{nv} - 2), \quad (10)$$

$$A^{\rm eff}_{nv} = A_{nv} + \gamma_{SRnv}\lambda_{nv}/(\lambda_{nv} - 2), \quad (11)$$

$$A^{\rm eff}_{Dnv} = A_{Dnv} - 2\gamma_{SRnv}/(\lambda_{nv} - 2), \quad (12)$$

where

$$\lambda_{nv} = A_{nv}/B_{nv}.$$

The spin–oribit coupling constant A of the $X^2\Pi$ ground state has been estimated by Brown *et al.* (*9*) as -2330 cm^{-1}. In view of the close agreement (within a few

[1] Equation (8) corrects an unfortunate misprint in the sign factor of the magnetic hyperfine term in Eq. (4) of Ref. (*14*).

percent) of their estimates for BrO and ClO with recent experimental values (*29, 30*), this value looks quite reliable. Although the value of A for the excited $A^2\Pi$ state is unknown, it is reasonable to assume it is large as well, like in ClO (*31*). As the B values are in the order of 0.3 cm^{-1}, the values of λ are large. The spin–rotation coupling constant γ_{SR} may be estimated from A (*32*) to be smaller than 1 GHz in case of the $X^2\Pi$ ground state, corresponding to a contribution to A_D^{eff} of less than 0.3 MHz. If the spin–orbit separation is not negligible compared with the vibrational interval, an additional correction must be added to A_D (*33*). However, this correction is in the order of 10 kHz for the $X^2\Pi$ ground state and can be neglected.

All the spectroscopic data on IO belong to the $A^2\Pi_{3/2}$–$X^2\Pi_{3/2}$ system only, which imposes further limitations on the determination of molecular constants and only allows the evaluation of effective parameters. For G_{nv} and A_{nv} the usual expansions as a series in v + (1/2) are applied

$$G_{nv} = \omega_{en}\left(v + \frac{1}{2}\right) - \omega_e x_{en}\left(v + \frac{1}{2}\right)^2, \tag{13}$$

$$A_{nv} = A_{en} - \alpha_{An}\left(v + \frac{1}{2}\right) + \gamma_{An}\left(v + \frac{1}{2}\right)^2. \tag{14}$$

For the $^2\Pi_{3/2}$ state (see Eq. (5)) the contributions from γ_{SRnv} in Eq. (10) and (11) cancel and the term $(1/2)A_{en}$ may be absorbed into an effective T_{ne}^{eff} ($^2\Pi_{3/2}$). The following effective vibrational parameters are obtained for G_{nv}^{eff} ($^2\Pi_{3/2}$)

$$\omega_{en}^{eff}(^2\Pi_{3/2}) = \omega_{en} - \frac{1}{2}\alpha_{An}, \tag{15}$$

$$\omega_e x_{en}^{eff}(^2\Pi_{3/2}) = \omega_e x_{en} - \frac{1}{2}\gamma_{An}. \tag{16}$$

Similarly the term A_{Dnv}^{eff} can be absorbed into an effective rotational constant, to a good approximation given by

$$B_{nv}^{eff}(^2\Pi_{3/2}) = B_{nv} + \frac{1}{2}A_{Dnv}^{eff}. \tag{17}$$

The value of $B_{nv}^{eff}(^2\Pi_{3/2})$ determined from the spectra depends only slightly on A_{nv}, because the off-diagonal term (see Eq. (6)) contributes after diagonalization by $B_{nv}/(\lambda_{nv} - 2)$, which is only -1.5 MHz for the $X^2\Pi$ ground state. Again, the usually applied vibrational expansion for B_{nv} has to be modified into an effective formulation,

$$B_{nv}^{eff}(^2\Pi_{3/2}) = B_{en}^{eff}(^2\Pi_{3/2}) - \alpha_{en}^{eff}(^2\Pi_{3/2})\left(v + \frac{1}{2}\right) + \gamma_{en}^{eff}(^2\Pi_{3/2})\left(v + \frac{1}{2}\right)^2, \tag{18}$$

where

$$B_{en}^{eff}(^2\Pi_{3/2}) = B_{en} + \frac{1}{2}A_{Den}^{eff}, \tag{19}$$

and $\alpha_{en}^{\text{eff}}(^2\Pi_{3/2})$ and $\gamma_{en}^{\text{eff}}(^2\Pi_{3/2})$ contain relatively small contributions from the vibrational dependence of A_{Dnv}^{eff} through Eq. (17). For the first-order centrifugal distortion parameter D_{nv}, the expansion

$$D_{nv} = D_{en} + \beta_{en}\left(v + \frac{1}{2}\right) \tag{20}$$

has been applied. The Λ-doubling for the $^2\Pi_{3/2}$ state arises purely via mixing with the $^2\Pi_{1/2}$ state. Its energy contributions can be approximated by $\pm(-1)^{J-1/2}(J - 1/2) \times (J + 1/2)(J + 3/2)q_{nv}^{\text{eff}}/(\lambda_{nv} - 2)$, where

$$q_{nv}^{\text{eff}} = q_{nv} + \left(\frac{1}{2}p_{nv} + q_{nv}\right)\Big/(\lambda_{nv} - 2), \tag{21}$$

giving rise to a very small splitting of the energy levels. In the pure precession approximation (*34*) the second term in Eq. (21) amounts half the magnitude of q_{nv} (because then $p_{nv} = \lambda_{nv}q_{nv}$).

The main features of the hyperfine structure are governed by the contributions from $a_{nv} + (1/2)(b_{nv} + c_{nv})$ and eQq_{1nv}. Smaller contributions arise from C_{1nv} and the off-diagonal term from b_{nv}. The latter two terms are totally correlated and do not allow an independent determination of C_{1nv} and b_{nv}. To a good approximation the contribution from C_{1nv} can be absorbed into the effective parameter

$$b_{nv}^{\text{eff}} = b_{nv} - C_{1nv}(\lambda_{nv} - 2). \tag{22}$$

The value of C_{1nv} may be roughly estimated as 50 kHz; thus both terms in the above equation give comparable contributions to b_{nv}^{eff} for IO. The small hyperfine Λ-doublet splittings depend mainly on the off-diagonal term eQq_{2nv}. Since the energy contributions of q_{nv}^{eff}, b_{nv}^{eff}, and eQq_{2nv} all arise purely from mixing with the $^2\Pi_{1/2}$ state, the values of these parameters determined from the spectra are proportional to $\lambda_{nv} - 2$ and thus depend strongly on the value of A_{nv}.

The excited $A^2\Pi_i$ states of the halogen monoxides exhibit extensive predissociation. The predissociation causes an additional decay path for the excited $A^2\Pi$ state, via interaction with unbound excited states. The total decay rate is then given by

$$\Gamma_{\text{tot}} = \Gamma_{\text{rad}} + \Gamma_{\text{pred}}, \tag{23}$$

where Γ_{rad} and Γ_{pred} denote the radiative and predissociative decay rates, respectively. Due to predissociation the lifetime of the excited state is shortened, which broadens the energy levels (to a width $\Delta\nu = \Gamma_{\text{tot}}/2\pi$) and diminishes the yield of spontaneous fluorescence emission (to a fraction $\Gamma_{\text{rad}}/\Gamma_{\text{tot}}$) in case of predissociation into nonfluorescent products (like ground state atoms). A survey on the nature of the coupling Hamiltonians with selection rules and dependence on the molecular quantum numbers in case of weak predissociation of a discrete excited level coupled to a continuum level, has been given by Vigué *et al.* (*35*). The radiative decay rate of the excited $A^2\Pi$ state of IO may be estimated from extrapolation of the corresponding electronic transition moment of ClO (*36*), giving $\Gamma_{\text{rad}} \sim 10^7$–$10^8$ sec^{-1} and $\Delta\nu_{\text{rad}} \sim$ 1–10 MHz.

Durie *et al.* (*6*) studied the $A^2\Pi_{3/2}$–$X^2\Pi_{3/2}$ transition of IO from flame emission spectra. They found that vibrational bands with $v' = 1$, 4, and 5 are completely diffuse, bands with $v' = 3$ are distinctly diffuse, and bands with $v' = 0$ and 2 have rotational lines which are sharp. The widths of rotational levels in the excited $v = 2$, $A^2\Pi_{3/2}$ state have been observed in the present experiment.

4. RESULTS AND ANALYSIS

The spectral line profile in the MBLE experiments is a convolution of a Lorentzian profile (natural linewidth, homogeneous line broadening) and a Gaussian profile (instrumental resolution, inhomogeneous line broadening), which results in a Voigt profile with a total linewidth $\Delta\nu_V$. The Gaussian contribution has an estimated linewidth (FWHM) $\Delta\nu_G$ of 10–20 MHz (Sect. 2). The Lorentzian contribution with a linewidth $\Delta\nu_L$ arises from the finite lifetime of the excited state, which is determined by the radiative and the predissociative decay times. The transitions studied terminate in the less predissociative vibrational level ($v = 2$) of the $A^2\Pi_{3/2}$ state, and the observed natural linewidths increase from 148 MHz ($J = 3/2$) up to about 2 GHz ($J = 49/2$). Since there is no analytical expression for the Voigt profile, numerical evaluation is required. Fortunately, in our case the Lorentzian contribution dominates. Because evaluation of Lorentzian profiles consumes much less computer time, a Lorentzian rather than a Voigt profile has been fitted by a least-squares method to the experimentally observed lineshape. For the most unfavorable case (with the smallest linewidth of 148 MHz) its adequacy in describing the Voigt profile has been checked, by fitting it to the corresponding Voigt profile, generated by a computational method (*37*). The overall agreement is good (within 0.1% of the central line intensity) and fully legitimates the use of Lorentzian profiles for data reduction from our spectra. The linewidth $\Delta\nu_L$ of the Lorentzian contribution can be extracted from the observed total linewidth $\Delta\nu_V$, with an accuracy better than 0.5%, by the approximated composition rule (*38*)

$$\Delta\nu_L = \Delta\nu_V[1 - (\Delta\nu_G/\Delta\nu_V)^2]. \tag{24}$$

The spectral recordings have been digitized in order to facilitate data reduction by a computer program. The resolved hyperfine structures of the lowest rotational transitions have been identified and analyzed first. The individual line centers and intensities of the hyperfine components of a given rotational transition were varied in the fitting procedure, together with a single linewidth for all the components. If the hyperfine components were allowed to have individually different linewidths, no significant variation was found within the experimental uncertainty.

The hyperfine structure could not be resolved for the higher rotational transitions and these spectra have been analyzed in a different way. The hyperfine pattern of a given rotational transition was fully calculated, using the diagonal hyperfine constants eQq_1 and $a + (1/2)(b + c)$ determined from the lowest rotational transitions and calculated relative intensities (*39*). Then, only the frequency of the hyperfine-free origin and the single linewidth of the hyperfine components were varied in the fit. In this procedure the Λ-doubling effects were neglected, as no indication of Λ-doubling splittings was noticed in the spectra. This is not unexpected, since the Λ-doubling

splitting in the $X^2\Pi_{3/2}$ state for the highest observed rotational level ($J = 51/2$) is calculated to be less than 0.5 MHz and it is reasonable to assume the Λ-doubling splitting in the $A^2\Pi_{3/2}$ state to be in the same order of magnitude.

In principle the Lorentzian linewidth contains homogeneous broadening contributions caused by collisions and saturation. Collision broadening can be excluded in view of the collision-free condition in the molecular beam. Saturation broadening increases the linewidth by the factor $(1 + S)^{1/2}$, wherein the saturation parameter S is the ratio of the induced emission rate to the total relaxation rate. By reducing the applied laser power it was experimentally verified that saturation effects can also be excluded. It was found that the fluorescence intensity decreased proportionally and the observed linewidths remained unchanged within the experimental uncertainty. Moreover, at the applied laser intensities of less than 1.5 mW/mm^2, the value of S can be estimated to be smaller than 10^{-3}.

The accuracy of the frequency interval measurements is in the order of 10 MHz, within a single laser scan. The absolute accuracy, and thus the relative accuracy of different scans, is in the order of 70 MHz. The accuracy of the linewidth measurements is about 10%. The measurements of the rf transition frequencies in the MODRES experiments have an accuracy in the order of 10 kHz.

The frequencies of transitions from the $A^2\Pi_{3/2}$–$X^2\Pi_{3/2}$ system of IO, observed in the present study, are given in Tables I, II, and III. The MBLE spectra are arranged in three groups corresponding to the 2–0, 2–1, and 2–2 vibrational bands, and are given in Tables I and II. Table I contains frequency intervals between hyperfine transitions, with unresolved Λ-doublet splittings, ($|\Delta F| = 0$, 1 and $- \leftarrow +$, $+ \leftarrow -$) and frequency intervals between hyperfine-free origins of rotational transitions ($|\Delta J| = 0$, 1 and $- \leftarrow +$, $+ \leftarrow -$). In Table II absolute frequencies of rotational transitions are given. The rf transitions in the $X^2\Pi_{3/2}$, $v = 0$ ground state observed by the MODRES method are listed in Table III. These hyperfine transitions are of the type $\Delta J = 0$, $|\Delta F| = 1$ and symmetry $- \leftrightarrow +$ or $+ \leftrightarrow -$.

The data set allows an unambiguous assignment of the quantum numbers involved and electronic state characterizations, with the exception of the vibrational quantum number $v = 2$ in the excited $A^2\Pi_{3/2}$ state that has been given in accordance with earlier investigations (see, e.g., Ref. (*6*)). The spectral line intensities are governed by the transition moments, the degree of predissociation, and the population of energy levels in the ground state. Using the Franck–Condon factors calculated by Rao *et al.* (*40*), the vibrational temperature in the IO beam was roughly estimated from relative intensity measurements to be 600 K.

The molecular parameters of IO have been determined in a least-squares fit of the calculated to the observed spectra, merging the results of the present study with those already existing in the literature. The present data on the 2–0 vibrational band of the $A^2\Pi_{3/2}$–$X^2\Pi_{3/2}$ spectrum and the $X^2\Pi_{3/2}$, $v = 0$ ground state were fitted, combined with the $X^2\Pi_{3/2}$, $v = 0$ microwave absorption data of Saito (*10*) and the 2–0, $A^2\Pi_{3/2}$–$X^2\Pi_{3/2}$ flame emission data of Durie *et al.* (*6*). In view of small internal inconsistencies in the microwave absorption data, as can be judged from discrepancies in sum and difference intercombination rules, the quoted errors had to be enlarged three times. The data of Durie *et al.* are consistent within an accuracy of 0.02 cm^{-1}, with the exception of two lines ($P(39.5)$ and $R(58.5)$) which deviate more than three

TABLE I

Observed and Calculated Frequency Intervals (MHz) between Hyperfine Transitions and between Hyperfine-Free Origins of Rotational Transitions in Vibrational Bands of the $A^2\Pi_{3/2}$–$X^2\Pi_{3/2}$ Spectrum of IO

Vib. band	F'	F"	Rot. trans.		F'	F"	Rot. trans.	Observed value	Obs. error	Obs. - calc.
2-0	4	3	Q(1.5)	-	4	4	Q(1.5)	637.2	4.8	-3.5
	3	2	Q(1.5)	-	4	4	Q(1.5)	-147.3	4.6	2.5
	2	1	Q(1.5)	-	4	4	Q(1.5)	-835.8	5.8	4.2
	3	3	Q(1.5)	-	4	4	Q(1.5)	-1 022.8	6.4	1.2
	3	4	Q(1.5)	-	4	4	Q(1.5)	-1 665.6	4.8	-1.0
	1	1	Q(1.5)	-	4	4	Q(1.5)	-1 898.0	11.7	2.1
	2	3	Q(1.5)	-	4	4	Q(1.5)	-2 476.0	3.9	1.3
	1	2	Q(1.5)	-	4	4	Q(1.5)	-2 662.9	5.6	0.4
	4	4	P(2.5)	-	4	5	P(2.5)	584.0	9.9	-0.9
	3	3	P(2.5)	-	4	5	P(2.5)	-696.4	6.7	-2.1
	3	4	P(2.5)	-	4	5	P(2.5)	-1 081.6	3.1	-1.9
	2	1	P(2.5)	-	4	5	P(2.5)	-1 752.5	30.8	-0.4
	2	2	P(2.5)	-	4	5	P(2.5)	-1 898.5	8.4	3.0
	2	3	P(2.5)	-	4	5	P(2.5)	-2 145.5	5.4	2.2
	1	1	P(2.5)	-	4	5	P(2.5)	-2 806.5	18.2	5.6
	1	2	P(2.5)	-	4	5	P(2.5)	-2 957.5	16.6	4.0
	5	5	P(3.5)	-	5	6	P(3.5)	526.1	19.4	-3.1
	4	4	P(3.5)	-	5	6	P(3.5)	-186.9	11.7	-2.2
	4	5	P(3.5)	-	5	6	P(3.5)	-472.3	3.2	0.1
	3	3	P(3.5)	-	5	6	P(3.5)	-806.2	11.5	-2.7
	3	4	P(3.5)	-	5	6	P(3.5)	-947.4	4.6	-6.2
	2	2	P(3.5)	-	5	6	P(3.5)	-1 323.7	16.7	-6.1
	2	3	P(3.5)	-	5	6	P(3.5)	-1 366.0	7.7	-3.9
	1	1	P(3.5)	-	5	6	P(3.5)	-1 688.4	10.1	-8.3
	1	2	P(3.5)	-	5	6	P(3.5)	-1 688.4	10.1	-3.8
	0	1	P(3.5)	-	5	6	P(3.5)	-1 871.8	30.1	-7.7
			R(1.5)	-			R(5.5)	1 560.3	20.0	-5.7
			R(4.5)	-			R(5.5)	6 600.0	18.0	-4.2
			R(2.5)	-			R(5.5)	7 381.0	20.0	-6.0
			R(3.5)	-			R(5.5)	9 063.6	17.0	-2.9
			Q(2.5)	-			R(8.5)	-4 571.4	14.0	-19.8
			Q(1.5)	-			R(8.5)	5 781.4	14.0	-18.5
			Q(3.5)	-			R(9.5)	4 136.5	23.0	5.3
			P(2.5)	-			R(10.5)	5 486.8	14.0	-21.3
			P(3.5)	-			R(11.5)	6 310.9	16.0	5.6
			P(4.5)	-			R(12.5)	7 120.4	13.0	13.8
			P(5.5)	-			R(13.5)	7 901.1	16.0	-11.4
			P(6.5)	-			R(14.5)	8 722.2	14.0	-1.4
			P(7.5)	-			R(15.5)	9 557.2	16.0	17.0
			P(8.5)	-			R(16.5)	10 362.7	19.0	-0.4
			P(9.5)	-			R(17.5)	11 193.0	23.0	0.4
			P(10.5)	-			R(18.5)	12 031.0	19.0	1.8
			P(11.5)	-			R(19.5)	12 883.8	21.0	10.4
			P(12.5)	-			R(20.5)	13 754.2	19.0	28.4
			P(13.5)	-			R(21.5)	14 536.9	42.0	-49.9
			P(14.5)	-			R(22.5)	15 414.0	53.0	-43.0
			P(15.5)	-			R(23.5)	16 330.1	29.0	-6.6
2-1	4	3	Q(1.5)	-	3	4	Q(1.5)	2 286.1	7.9	-1.7
	1	1	Q(1.5)	-	3	4	Q(1.5)	-258.1	10.2	-0.2
	2	3	Q(1.5)	-	3	4	Q(1.5)	-830.5	5.3	-0.5
	1	2	Q(1.5)	-	3	4	Q(1.5)	-1 021.8	7.6	-0.8
	4	4	P(2.5)	-	4	5	P(2.5)	579.0	9.3	-0.8
	3	3	P(2.5)	-	4	5	P(2.5)	-705.0	7.9	-0.1
	3	4	P(2.5)	-	4	5	P(2.5)	-1 086.9	3.7	-2.1
	2	1	P(2.5)	-	4	5	P(2.5)	-1 757.9	34.0	13.0
	2	2	P(2.5)	-	4	5	P(2.5)	-1 915.4	11.6	1.3
	2	3	P(2.5)	-	4	5	P(2.5)	-2 154.8	7.4	3.3
	1	1	P(2.5)	-	4	5	P(2.5)	-2 819.7	31.4	10.9
	1	2	P(2.5)	-	4	5	P(2.5)	-2 972.4	21.0	4.1
	5	5	P(3.5)	-	4	5	P(3.5)	1 001.1	19.7	-0.3
	5	6	P(3.5)	-	4	5	P(3.5)	471.5	3.8	-1.0
	4	4	P(3.5)	-	4	5	P(3.5)	282.6	15.9	-1.6
	3	3	P(3.5)	-	4	5	P(3.5)	-346.1	11.7	-1.1
	3	4	P(3.5)	-	4	5	P(3.5)	-474.8	5.6	-2.3
	2	2	P(3.5)	-	4	5	P(3.5)	-850.0	22.6	8.9

TABLE I—*Continued*

Vib. band	F'	F''	Rot. trans.		F'	F''	Rot. trans.	Observed value	Obs. error	Obs. - calc.
	2	3	P(3.5)	-	4	5	P(3.5)	-899.5	9.7	-1.2
	1	1	P(3.5)	-	4	5	P(3.5)	-1 223.0	9.2	2.3
	1	2	P(3.5)	-	4	5	P(3.5)	-1 223.0	9.2	2.9
	0	1	P(3.5)	-	4	5	P(3.5)	-1 409.5	20.7	-0.1
			R(1.5)	-			R(6.5)	8 646.8	19.0	1.9
			R(5.5)	-			R(6.5)	9 695.5	14.0	8.5
			R(2.5)	-			R(6.5)	14 886.9	18.0	13.5
			R(4.5)	-			R(6.5)	15 408.2	16.0	13.5
			R(3.5)	-			R(6.5)	17 135.6	16.0	12.1
			Q(1.5)	-			Q(2.5)	9 935.6	25.0	-8.4
			R(8.5)	-			Q(2.5)	10 423.5	42.0	4.0
			Q(3.5)	-			R(9.5)	-2 693.3	27.0	21.2
			P(2.5)	-			R(10.5)	-3 645.2	21.0	-25.8
			P(3.5)	-			R(11.5)	-4 133.4	17.0	-7.5
			P(4.5)	-			R(12.5)	-4 629.0	20.0	-0.7
			P(5.5)	-			R(13.5)	-5 131.4	19.0	-5.2
			R(14.5)	-			P(6.5)	5 615.1	14.0	-4.1
			R(15.5)	-			P(7.5)	6 109.9	13.0	3.0
			R(16.5)	-			P(8.5)	6 588.7	17.0	-0.2
			R(17.5)	-			P(9.5)	7 032.3	24.0	-32.7
			R(18.5)	-			P(10.5)	7 547.1	18.0	12.3
2-2	4	3	Q(1.5)	-	4	4	Q(1.5)	628.9	12.5	16.7
	3	2	Q(1.5)	-	4	4	Q(1.5)	-196.4	12.0	-1.9
	2	1	Q(1.5)	-	4	4	Q(1.5)	-894.2	16.3	-1.7
	3	3	Q(1.5)	-	4	4	Q(1.5)	-1 068.3	19.6	-15.5
	3	4	Q(1.5)	-	4	4	Q(1.5)	-1 671.8	14.1	-6.8
	1	1	Q(1.5)	-	4	4	Q(1.5)	-1 965.7	35.6	-13.4
	2	3	Q(1.5)	-	4	4	Q(1.5)	-2 518.5	14.4	-12.5
	1	2	Q(1.5)	-	4	4	Q(1.5)	-2 706.0	22.0	1.4
	4	4	P(2.5)	-	4	5	P(2.5)	579.8	19.0	7.1
	3	3	P(2.5)	-	4	5	P(2.5)	-714.5	15.8	3.1
	3	4	P(2.5)	-	4	5	P(2.5)	-1 085.1	12.7	7.3
	2	2	P(2.5)	-	4	5	P(2.5)	-1 925.5	14.4	7.7
	2	3	P(2.5)	-	4	5	P(2.5)	-2 179.3	13.6	-8.5
			R(1.5)	-			R(5.5)	-3 688.1	24.0	-26.9
			R(2.5)	-			R(5.5)	2 967.0	19.0	-9.5
			R(4.5)	-			R(5.5)	4 800.8	17.0	-6.5
			R(3.5)	-			R(5.5)	5 791.7	16.0	-7.7
			Q(1.5)	-			R(8.5)	-6 804.3	19.0	-25.2
			Q(2.5)	-			R(9.5)	3 734.5	24.0	-22.0
			P(2.5)	-			R(10.5)	-12 824.7	19.0	-34.6
			P(3.5)	-			R(11.5)	-14 612.6	21.0	-4.5

times this error and were consequently rejected from the fit. The results of this fit determine the molecular parameters in the $A^2\Pi_{3/2}$, $v = 2$ and $X^2\Pi_{3/2}$, $v = 0$ states.

The present data on the 2–1 vibrational band of the $A^2\Pi_{3/2}$–$X^2\Pi_{3/2}$ spectrum were fitted with the excited state parameters constrained within their uncertainty to their values obtained from the 2–0 band. This is done as the 2–0 band yields the most accurate parameters for the $A^2\Pi_{3/2}$, $v = 2$ state. The present data on the 2–2 vibrational band of the $A^2\Pi_{3/2}$–$X^2\Pi_{3/2}$ spectrum were fitted, combined with the 2–2, $A^2\Pi_{3/2}$–$X^2\Pi_{3/2}$ emission data of Durie *et al.* and with the excited state parameters again constrained to the results of the 2–0 band. Again, some lines of the data of Durie *et al.* had to be rejected ($R(66.5)$, $R(68.5)$, $R(75.5)$, $R(77.5)$, $P(64.5)$, $P(65.5)$, $P(67.5)$, $P(68.5)$, and $P(69.5)$), while the consistency was greatly improved by lowering their absolute frequencies for the 2–2 band by 0.03 cm^{-1}. The final molecular parameters

TABLE II

Observed and Calculated Absolute Frequencies (cm^{-1}) of Hyperfine-Free Origins of Rotational Transitions in Vibrational Bands of the $A^2\Pi_{3/2}$–$X^2\Pi_{3/2}$ Spectrum of IO

Vib. band	Rot. trans.	Observed value	Obs. error	Obs. - calc.
2-0	R(5.5)	22 471.0987	0.0027	-0.0010
	R(6.5)	22 470.7411	0.0025	-0.0002
	R(7.5)	22 470.2432	0.0025	-0.0014
	R(8.5)	22 469.6091	0.0025	-0.0007
	R(9.5)	22 468.8348	0.0025	-0.0019
	R(10.5)	22 467.9245	0.0025	-0.0010
	R(11.5)	22 466.8751	0.0025	-0.0010
	P(4.5)	22 465.9255	0.0025	0.0001
	P(5.5)	22 464.6279	0.0025	0.0015
	P(6.5)	22 463.1910	0.0025	0.0017
	P(7.5)	22 461.6168	0.0025	0.0027
	P(8.5)	22 459.9013	0.0025	0.0004
	P(9.5)	22 458.0501	0.0025	0.0005
	P(10.5)	22 456.0593	0.0025	-0.0010
	P(11.5)	22 453.9334	0.0025	0.0004
	P(12.5)	22 451.6671	0.0025	-0.0005
	P(13.5)	22 449.2640	0.0025	-0.0002
	P(14.5)	22 446.7244	0.0025	0.0016
	P(15.5)	22 444.0426	0.0025	-0.0008
	P(16.5)	22 441.2267	0.0025	0.0007
	P(17.5)	22 438.2707	0.0025	0.0001
	P(18.5)	22 435.1759	0.0025	-0.0014
	P(19.5)	22 431.9444	0.0029	-0.0015
	P(20.5)	22 428.5783	0.0030	0.0017
	P(21.5)	22 425.0681	0.0029	-0.0013
	P(22.5)	22 421.4239	0.0031	-0.0003
	P(23.5)	22 417.6421	0.0028	0.0011
	P(24.5)	22 413.7195	0.0029	-0.0004
	P(25.5)	22 409.6603	0.0029	-0.0007
2-1	R(6.5)	21 798.0112	0.0024	0.0001
	R(7.5)	21 797.5568	0.0024	0.0016
	Q(2.5)	21 796.6189	0.0025	-0.0001
	R(9.5)	21 796.2448	0.0024	-0.0004
	R(10.5)	21 795.3899	0.0024	-0.0011
	R(11.5)	21 794.4030	0.0024	-0.0011
	R(12.5)	21 793.2843	0.0024	-0.0001
	R(13.5)	21 792.0302	0.0025	-0.0017
	P(6.5)	21 790.4583	0.0024	-0.0008
	P(7.5)	21 788.9249	0.0024	0.0002
	P(8.5)	21 787.2573	0.0024	-0.0004
	P(9.5)	21 785.4584	0.0025	0.0003
	P(10.5)	21 783.5281	0.0024	0.0022
	P(11.5)	21 781.4613	0.0024	0.0002
	P(12.5)	21 779.2637	0.0024	0.0000
	P(13.5)	21 776.9345	0.0024	0.0008
	P(14.5)	21 774.4718	0.0024	0.0006
	P(15.5)	21 771.8764	0.0026	0.0002
	P(16.5)	21 769.1486	0.0024	0.0000
	P(17.5)	21 766.2885	0.0024	-0.0000
	P(18.5)	21 763.2954	0.0024	-0.0005
2-2	R(5.5)	21 134.3115	0.0024	0.0027
	R(6.5)	21 134.0236	0.0024	0.0025
	R(7.5)	21 133.6101	0.0024	0.0039
	R(8.5)	21 133.0650	0.0024	0.0010
	R(9.5)	21 132.3960	0.0024	0.0014
	R(10.5)	21 131.5989	0.0024	0.0011
	R(11.5)	21 130.6744	0.0024	0.0007
	R(12.5)	21 129.6228	0.0024	0.0005
	P(4.5)	21 129.0727	0.0024	-0.0018
	R(13.5)	21 128.4423	0.0024	-0.0013
	P(5.5)	21 127.8340	0.0024	-0.0014
	R(14.5)	21 127.1344	0.0024	-0.0031
	P(6.5)	21 126.4680	0.0024	-0.0011
	P(7.5)	21 124.9753	0.0024	-0.0003
	P(8.5)	21 123.3533	0.0024	-0.0017
	P(9.5)	21 121.6057	0.0024	-0.0015
	P(10.5)	21 119.7322	0.0024	-0.0001
	P(11.5)	21 117.7303	0.0024	0.0001
	P(12.5)	21 115.6013	0.0024	0.0003
	P(13.5)	21 113.3443	0.0024	-0.0004

TABLE III

Observed and Calculated Frequencies (MHz) of Hyperfine Transitions in the $v = 0$, $X^2\Pi_{3/2}$ Ground State of IO

F'	F''	Rot. trans.	Observed value	Obs. error	Obs. - calc.
4_-	3_+	Q(1.5)	640.767	0.030	-0.004
4_-	3_+	Q(2.5)	385.716	0.015	0.004
5_+	4_-	Q(3.5)	288.129	0.010	-0.002
5_-	4_+	Q(3.5)	287.294	0.010	-0.000
6_-	5_+	Q(4.5)	249.211	0.006	0.000
6_+	5_-	Q(4.5)	248.179	0.008	0.000

of IO are given in Table IV. Since the present results are more accurate and contain additional information and because data from previous studies have been included, a comparison with former results is not meaningful.

TABLE IV

Molecular Parameters of IO (all values are in MHz, unless otherwise indicated; the errors correspond to three standard deviations)

	$X^2\Pi_{3/2}$ state			$A^2\Pi_{3/2}$ state
	v = 0	v = 1	v = 2	v = 2
A_{nv}^{eff} (cm^{-1})[a]	-2 330	-2 330	-2 330	-2 330
$B_{nv}^{eff}(^2\Pi_{3/2})$	10 158.586(35)	10 077.05(29)	9 995.25(25)	8 087.76(12)
D_{nv}	0.01021(75)	0.0101(20)	0.00943(72)	0.00945(69)
H_{nv}	$-0.09(31)\times10^{-6}$	$-1.2(4.8)\times10^{-6}$	$-0.21(15)\times10^{-6}$	$-0.19(13)\times10^{-6}$
q_{nv}^{eff}	0.3(1.2)			
$a_{nv}+\frac{1}{2}(b_{nv}+c_{nv})$	583.832(95)	576.7(1.8)	568.8(5.5)	1 138.2(1.5)
b_{nv}^{eff}	660(68)			
eQq_{1nv}	-1 894.75(91)	-1 932(24)	-1 921(115)	-1 078(23)
eQq_{2nv}	-3 808(298)			
$\nu_{0\ 2\text{-}v}^{A\text{-}X}$ (cm^{-1})[b]	22 470.0104(25)	21 797.1497(24)	21 133.0288(26)	

[a] Parameter constrained at this value (see text).

[b] Band origins of the 2-v vibrational bands of the $A^2\Pi_{3/2}$-$X^2\Pi_{3/2}$ spectrum.

The observed natural widths $\Delta\nu$ of the rotational states in the $v = 2$ vibrational level of the excited $A^2\Pi_{3/2}$ state are presented as a function of $J(J + 1)$ in Fig. 6. The widths consist of inseparable radiative and predissociative parts (Eq. (23)). As the radiative width was estimated as 1–10 MHz (Sect. 3), the predissociation rate exceeds the radiation rate by several orders of magnitude. The variation of the lifetime τ in the $v = 2$ level of the excited state can be described well by

$$1/\tau = 1/\tau_0 + kJ(J + 1), \tag{25}$$

where τ_0 denotes the extrapolated lifetime of the rotation-free state. The following values have been determined: $\tau_0 = 1.21(12)$ nsec (corresponding to the width $\Delta\nu_0 = 132(13)$ MHz) and $k = 1.72(16) \times 10^7$ sec^{-1}.

Attempts to observe MBLE spectra to other vibrational levels in the excited $A^2\Pi_{3/2}$ state (concentrated on the 0–0 and 3–0 vibrational bands) were not successful. The stronger predissociation in the excited $v = 3$ level (*6*) and the low Franck–Condon factor of the 0–0 band (*40*) most probably account for this. Attempts to observe rf transitions in the $v = 0$, $X^2\Pi_{3/2}$ ground state by conventional MBER spectroscopy or to observe laser excitation spectra through the subsequent (photo) dissociation, both by means of beam detection with a mass spectrometer, failed as well. This demonstrates the higher sensitivity of laser-induced fluorescence detection.

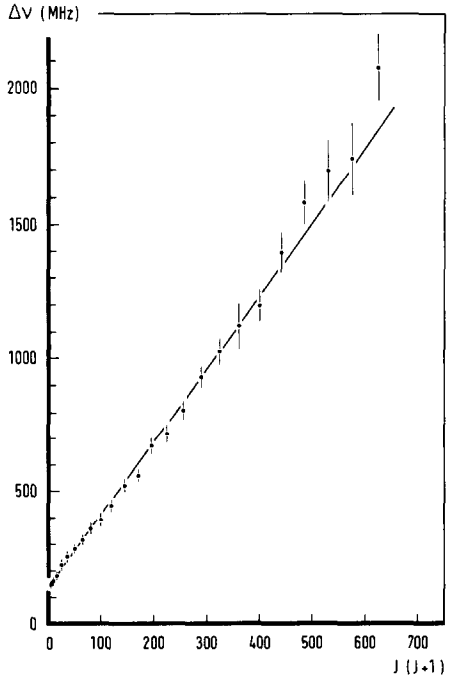

FIG. 6. Observed natural widths (FWHM) $\Delta\nu$ of the rotational states in the $v = 2$ vibrational level of the excited $A^2\Pi_{3/2}$ state of IO, plotted as a function of $J(J + 1)$.

5. DISCUSSION

All the spin–orbit coupling constants A have been constrained at the estimated value of $-2330\ cm^{-1}$ (*9*). The indicated errors do not reflect uncertainty in these A values. The dependence of the determined parameters on the A values has been discussed in Section 3. Vibrational effects in A_{Xv} can be expected to be negligible compared to the accuracy of the $B^{eff}_{Xv}(^2\Pi_{3/2})$ values. However, the unknown spin–orbit coupling constant A_{Av} in the excited $A^2\Pi_{3/2}$ state has a large impact on the uncertainty of the $B^{eff}_{A2}(^2\Pi_{3/2})$ value. The maximum deviation of $B^{eff}_{A2}(^2\Pi_{3/2})$ is 14 MHz for a value of $|\lambda_{A2}|$ larger than 900. The following effective internuclear distances are obtained from the corresponding $B^{eff}_{nv}(^2\Pi_{3/2})$ values: $r^{eff}_{X0}(^2\Pi_{3/2})$ = 0.1871448(19) nm, $r^{eff}_{X1}(^2\Pi_{3/2})$ = 0.1879004(32) nm, $r^{eff}_{X2}(^2\Pi_{3/2})$ = 0.1886677(30) nm, and $r^{eff}_{A2}(^2\Pi_{3/2})$ = 0.20974(18) nm. The stated errors in $r^{eff}_{nv}(^2\Pi_{3/2})$ also reflect the estimated uncertainty in the A_{nv} values.

The present data cover the three lowest vibrational levels of the ground state and allow vibrational expansion of the molecular constants. The results for the $X^2\Pi_{3/2}$ state are given in Table V. The values of $\omega^{eff}_{eX}(^2\Pi_{3/2})$ and $\omega_e x^{eff}_{eX}(^2\Pi_{3/2})$ in Table V have been derived from an expansion up to second order in $v + (1/2)$, because the present data are limited to two vibrational intervals. If the third-order coefficient

TABLE V

Derived Molecular Constants for the $X^2\Pi$ Ground State of IO
(the errors correspond to three standard deviations)

Constant	Value	Unit
$\omega^{eff}_{eX}(^2\Pi_{3/2})$ [a]	681.6004(91)	cm^{-1}
$\omega_e x^{eff}_{eX}(^2\Pi_{3/2})$ [a]	4.3699(30)	cm^{-1}
$B^{eff}_{eX}(^2\Pi_{3/2})$	10 199.25(46)	MHz
$\alpha^{eff}_{eX}(^2\Pi_{3/2})$	81.27(91)	MHz
$\gamma^{eff}_{eX}(^2\Pi_{3/2})$	-0.13(32)	MHz
D_{eX}	0.01042(66)	MHz
β_{eX}	-0.00038(51)	MHz
$r^{eff}_{eX}(^2\Pi_{3/2})$	0.1867713(46)	nm
ω_{eX} [b]	669.7(2.4)	cm^{-1}
B_{eX} [c]	10 083(24)	MHz
r_{eX} [c]	0.18784(22)	nm

[a] Derived from an expansion up to second order in $v+\frac{1}{2}$.

[b] Derived using the estimated α_{AX}=-23.8(4.8) cm^{-1} (see text).

[c] Derived using the estimated A_{DeX}=233(47) cm^{-1} (see text).

$\omega_e y_{eX}^{eff}(^2\Pi_{3/2})$ determined as -0.01_3 MHz by Durie *et al.* (*6*) is included, the values of $\omega_{eX}^{eff}(^2\Pi_{3/2})$ and $\omega_e x_{eX}^{eff}(^2\Pi_{3/2})$ have to be changed by $+5.75\omega_e y_{eX}^{eff}(^2\Pi_{3/2})$ $(= -0.08\ cm^{-1})$ and $+4.5\omega_e y_{eX}^{eff}(^2\Pi_{3/2})$ $(= -0.06\ cm^{-1})$, respectively. The equilibrium values for ω, B, and r have been deduced from the effective constants in the following way. If it is assumed that the vibrational effect in A_{Xv} in ClO (1.02% (*30*)) and IO are equal to within 20%, the coefficient α_{AX} of IO can be estimated to be $-23.8(4.8)\ cm^{-1}$. The vibrational frequency ω_{eX} is then obtained from Eq. (15). Assuming the ratio A_{DX}/A_X in IO to be equal to within 20% to these ratios in ClO (*30*) and BrO (*29*), the A_{DeX} value for IO can be estimated as 233(47) MHz. Eq. (19) yields the equilibrium rotational constant B_{eX} and the corresponding equilibrium internuclear distance r_{eX}. The results are given in Table V. Alternatively, the well-known relation (valid for a Morse potential)

$$\omega_{en}^2 = 4B_{en}^3/D_{en} \tag{26}$$

may be applied. This yields $\omega_{eX} = 662(21)\ cm^{-1}$, where the error mainly results from the limited accuracy of D_{eX}. This value shows gratifying agreement with the corresponding value in Table V.

If the parameters in Eq. (26) are replaced by their effective values, the following relation between α_{An} and A_{Den} is obtained with the use of Eq. (15) and (19)

$$\alpha_{An} = -(4/D_{en}^{1/2})\left\{[B_{en}^{eff}(^2\Pi_{3/2})]^{3/2} - \left[B_{en}^{eff}(^2\Pi_{3/2}) - \frac{1}{2}A_{Den}\right]^{3/2}\right\}. \tag{27}$$

By substituting the values of $B_{eX}^{eff}(^2\Pi_{3/2})$ and D_{eX} determined from the spectra and the estimated A_{DeX} value in Eq. (27), $\alpha_{AX} = -23.0(4.8)\ cm^{-1}$ is obtained. This value agrees very well with the estimate of α_{AX} made above.

The lack of data on the $A^2\Pi_{1/2}$–$X^2\Pi_{1/2}$ system seriously limits the determination of all the molecular parameters. Especially, only an upper limit can be given for the Λ-doubling parameter q^{eff}. Determination of a complete set of magnetic hyperfine constants is also impeded.

The hyperfine constants are related to expectation values of electronic operators (*24*). The hyperfine constants in the $X^2\Pi$ ground state of ClO (*30*) BrO (*29, 41*) show that the electron distribution in the outer shell of both molecules is nearly identical with the unpaired π electron mainly located at the halogen atom. Particularly, the expectation values of $\langle \sin^2\theta/r^3\rangle_U$ derived from the d constant and the eQq_2 constant, show a good agreement: (in units of $10^{24}\ cm^{-3}$) 14.9 and 15.3, respectively, in the case of ClO and 28.0 and 27.4, respectively, in the case of BrO (see Appendix.) The electron distribution in the outer shell of IO is essentially identical to the ClO and BrO distributions. The d constant of IO can be estimated from the presently determined eQq_2 constant (−3808(298) MHz). This value yields $\langle \sin^2\theta/r^3\rangle_U = 46.1(3.6) \times 10^{24}$ cm^{-3}, which gives $d = 1099(110)$ MHz.

The vibrational effects in the $X^2\Pi_{3/2}$ ground state are about 1%. The excitation to the $A^2\Pi_{3/2}$ state involves a considerable change in the electron distribution, as can be noticed by large effects on the hyperfine constants, accompanied by an increase in the internuclear distance.

The predissociation rate of the $A^2\Pi_{3/2}$, $v = 2$ state has been found to be proportional to $J(J + 1)$. No significant dependence on the quantum number F was noticed and

both the + and − parity levels are predissociative to an equal extent as could be concluded from the double-resonance measurements. Until now, only vibrational dependence of the predissociation rate in the $A^2\Pi_i$ states has been reported for IO (*6*), BrO (*42*), and ClO (*43*). The nature of the interacting unbound state(s) is still subject to discussion. Recent calculations (*44*) have shown that presumably more than one interacting repulsive state is involved in case of ClO. The observed rotational dependence of the predissociation rate could in principle be due to a rotational variation of the Franck–Condon density for predissociation (centrifugal effect). However, this is not very likely in view of the rather strong variation observed. It seems more plausible that this variation originates from an additional gyroscopic interaction with unbound states. Accurate and complete measurements on the variation of the widths in the excited $A^2\Pi_i$ states of the halogen monoxides are desirable for understanding the predissociation.

6. CONCLUSIONS

The present study presents the first high-resolution investigation of the $A^2\Pi_{3/2}$–$X^2\Pi_{3/2}$ system of IO by means of laser-induced fluorescence. More accurate and new information about the molecular constants of IO has been obtained, summarized in Tables IV and V. The hyperfine interaction in the excited state and the hyperfine Λ-doublet splittings in the ground state have been observed for the first time.

Spectroscopic techniques based on laser-induced fluorescence are probably not suitable for application to the lighter halogen monoxides, which exhibit more extensive predissociation. Observation of the $A^2\Pi_{1/2}$–$X^2\Pi_{1/2}$ system of IO will also be hindered by low degree of population in the $X^2\Pi_{1/2}$ state as a consequence of the large fine-structure interval.

The new technique of microwave optical double resonance on an electrically state-selected beam (MODRES) presented in this paper has promising prospects for observations on the ground state spectra of polar molecules. Its high resolution and high sensitivity have been demonstrated in the experiments on the thermally populated and low concentration beam of the predissociative IO radical.

APPENDIX

The question of the sign of the nonaxial electric quadrupole coupling constant eQq_2 (see Eq. (9)) is connected to the problem of the choice of the phase factors for the off-diagonal matrix elements between the $^2\Pi_{1/2}$ and $^2\Pi_{3/2}$ states. The three major off-diagonal contributions arise from B, b, and eQq_2. The phase convention we used before (*24*) was introduced by Van Vleck (*34*) and is based on the reversed angular momentum method (*45, 46*). It resulted, however, in contradictory results for the value of $\langle \sin^2 \theta / r^3 \rangle_U$ derived from d and eQq_2 (see below). Recently Brown and Howard (*27*) established a consistent phase convention from the direct tensor method. When the off-diagonal matrix elements obtained from the direct tensor and reversed angular momentum methods are compared, the signs in front of B and b are to be reversed, while the sign in front of eQq_2 remains unaffected. Because the contributions of the off-diagonal matrix elements to the energy depend only on the relative signs, the sign of the eQq_2 value is consequently to be reversed. The phase convention

employed presently is in accordance with the direct tensor method. The present sign of eQq_2 is also in agreement with the physical interpretation of the hyperfine coupling constants, considering the mutual relations for d and q_2 (*24*):

$$d = (3/2)gg_I\mu_0\mu_N\langle \sin^2 \theta/r^3\rangle_U, \tag{A1}$$

$$q_2 = -3\langle \sin^2 \theta/r^3\rangle_T. \tag{A2}$$

Here U and T denote averaging over the unpaired electron and the total electron density, respectively. Equation (A2) can be rewritten in an effective average for the unpaired electron, in the case of a single π electron in the outer shell by

$$q_2[(n\pi)] = -3\langle \sin^2 \theta/r^3\rangle_U \tag{A3}$$

and, in the case of three equivalent π electrons, by

$$q_2[(n\pi)^3] = 3\langle \sin^2 \theta/r^3\rangle_U. \tag{A4}$$

The signs of $\langle \sin^2 \theta/r^3\rangle_U$ derived from the values of d and eQq_2, now agree (being both positive) in case of, for example, OD and SD (*24*), NO (*25*), CCl and ClO (*47*). For the halogen monoxides (three π electrons) ClO (*30, 48*) and BrO (*29, 41*),[2] both with positive d values, the corrected and consistent eQq_2 values are negative and positive, respectively. The d value of IO will be positive as well and consequently the eQq_2 value for IO is expected to be negative.

ACKNOWLEDGMENTS

The authors thank Mr. J. J. Holtkamp and Mr. C. A. Sikkens for their excellent technical assistance and Mr. W. M. van Herpen for his assistance during the experiments. Stimulating discussions with Dr. W. A. Majewski and Dr. J. J. Van Vaals are greatly appreciated.

RECEIVED: June 6, 1983

REFERENCES

1. W. L. CHAMEIDES AND D. D. DAVIS, *J. Geophys. Res.* **85,** 7383–7398 (1980).
2. A. R. W. MCKELLAR, *Canad. J. Phys.* **57,** 2106–2113 (1979).
3. W. M. VAIDYA, *Proc. Indian Acad. Sci. Sect. A* **6,** 122–128 (1937).
4. E. H. COLEMAN, A. G. GAYDON, AND W. M. VAIDYA, *Nature (London)* **162,** 108–109 (1948).
5. R. A. DURIE AND D. A. RAMSAY, *Canad. J. Phys.* **36,** 35–53 (1958).
6. R. A. DURIE, F. LEGAY, AND D. A. RAMSAY, *Canad. J. Phys.* **38,** 444–452 (1960).
7. A. LOEWENSCHUSS, J. C. MILLER, AND L. ANDREWS, *J. Mol. Spectrosc.* **80,** 351–362 (1980).
8. A. CARRINGTON, P. N. DYER, AND D. H. LEVY, *J. Chem. Phys.* **52,** 309–314 (1970).
9. J. M. BROWN, C. R. BYFLEET, B. J. HOWARD, AND D. K. RUSSELL, *Mol. Phys.* **23,** 457–468 (1972).
10. S. SAITO, *J. Mol. Spectrosc.* **48,** 530–535 (1973).
11. J. C. ZORN AND T. C. ENGLISH, *in* "Advances in Atomic and Molecular Physics" (D. Bates and I. Estermann, Eds.), Vol. 9, Academic Press, New York, 1973.
12. P. GRUNDEVIK, M. GUSTAVSSON, I. LINDGREN, G. OLSSON, L. ROBERTSSON, A. ROSÉN, AND S. SVANBERG, *Phys. Rev. Lett.* **42,** 1528–1531 (1979).
13. S. D. ROSNER, R. A. HOLT, AND T. D. GAILY, *Phys. Rev. Lett.* **35,** 785–789 (1975).
14. W. L. MEERTS, J. P. BEKOOY, AND A. DYMANUS, *Mol. Phys.* **37,** 425–439 (1979).

[2] Cohen *et al.* (*41*) obtained a positive value of eQq_2 for BrO due to an erroneous sign in their Eq. (15).

15. J. L. HALL AND S. A. LEE, *Appl. Phys. Lett.* **29,** 367–369 (1976).
16. F. V. KOWALSKI, R. T. HAWKINS, AND A. L. SCHAWLOW, *J. Opt. Soc. Amer.* **66,** 965–966 (1976).
17. F. V. KOWALSKI, R. E. TEETS, W. DEMTRÖDER, AND A. L. SCHAWLOW, *J. Opt. Soc. Amer.* **68,** 1611–1613 (1978).
18. R. BALHORN, H. KUNZMANN, AND F. LEBOWSKY, *Appl. Opt.* **11,** 742–744 (1972).
19. S. J. BENNETT, R. E. WARD, AND D. C. WILSON, *Appl. Opt.* **12,** 1406 (1973).
20. V. KAUFMAN, *J. Opt. Soc. Amer.* **52,** 866–870 (1962).
21. K. SHIMODA (Ed.), "High-Resolution Laser Spectroscopy, Topics in Applied Physics," Vol. 13, Springer-Verlag, Berlin/New York, 1976.
22. W. DEMTRÖDER, "Laser Spectroscopy, Springer Series in Chemical Physics," Vol. 5, Springer-Verlag, Berlin/New York, 1981.
23. C. R. BYFLEET, A. CARRINGTON, AND D. K. RUSSELL, *Mol. Phys.* **20,** 271–277 (1971).
24. W. L. MEERTS AND A. DYMANUS, *Canad. J. Phys.* **53,** 2123–2141 (1975).
25. W. L. MEERTS, *Chem. Phys.* **14,** 421–425 (1976).
26. J. M. BROWN, E. A. COLBOURN, J. K. G. WATSON, AND F. D. WAYNE, *J. Mol. Spectrosc.* **74,** 294–318 (1979).
27. J. M. BROWN AND B. J. HOWARD, *Mol. Phys.* **31,** 1517–1525 (1976).
28. C. AMIOT, J.-P. MAILLARD, AND J. CHAUVILLE, *J. Mol. Spectrosc.* **87,** 196–218 (1981).
29. A. R. W. MCKELLAR, *J. Mol. Spectrosc.* **86,** 43–54 (1981).
30. J. A. COXON, *Canad. J. Phys.* **57,** 1538–1552 (1979).
31. J. A. COXON, W. E. JONES, AND E. G. SKOLNIK, *Canad. J. Phys.* **54,** 1043–1052 (1976).
32. S. GREEN AND R. N. ZARE, *J. Mol. Spectrosc.* **64,** 217–222 (1977).
33. J. M. BROWN AND J. E. SCHUBERT, *J. Mol. Spectrosc.* **95,** 194–212 (1982).
34. J. H. VAN VLECK, *Phys. Rev.* **33,** 467–506 (1929).
35. J. VIGUÉ, M. BROYER, AND J. C. LEHMANN, *J. Phys. Colloq. Orsay Fr.* **42,** 937–947 (1981); *J. Phys. Colloq. Orsay Fr.* **42,** 949–959 (1981).
36. M. MANDELMAN AND R. W. NICHOLLS, *J. Quant. Spectrosc. Radiat. Transfer* **17,** 483–491 (1977).
37. B. H. ARMSTRONG, *J. Quant. Spectrosc. Radiat. Transfer* **7,** 61–88 (1967).
38. S. N. DOBRYAKOV AND YA. S. LEBEDEV, *Sov. Phys. Dokl. Engl. Transl.,* **13,** 873–875 (1969).
39. W. GORDY AND R. L. COOK, "Microwave Molecular Spectra," Interscience, New York, 1970.
40. M. L. P. RAO, D. V. K. RAO, AND P. T. RAO, *Phys. Lett. A* **50,** 341–342 (1974).
41. E. A. COHEN, H. M. PICKETT, AND M. GELLER, *J. Mol. Spectrosc.* **87,** 459–470 (1981).
42. M. BARNETT, E. A. COHEN, AND D. A. RAMSAY, *Canad. J. Phys.* **59,** 1908–1916 (1981).
43. J. A. COXON AND D. A. RAMSAY, *Canad. J. Phys.* **54,** 1034–1042 (1976).
44. P. R. BUNKER AND P. C. KLEIN, *Chem. Phys. Lett.* **78,** 552–554 (1981).
45. J. H. VAN VLECK, *Rev. Mod. Phys.* **23,** 213–227 (1951).
46. K. F. FREED, *J. Chem. Phys.* **45,** 4214–4241 (1966).
47. Y. ENDO, S. SAITO, AND E. HIROTA, *J. Mol. Spectrosc.* **92,** 443–450 (1982); *J. Mol. Spectrosc.* **94,** 199–207 (1982).
48. R. K. KAKAR, E. A. COHEN, AND M. GELLER, *J. Mol. Spectrosc.* **70,** 243–256 (1978).